Figure S1. Evaluation of hPSC-derived signaling center

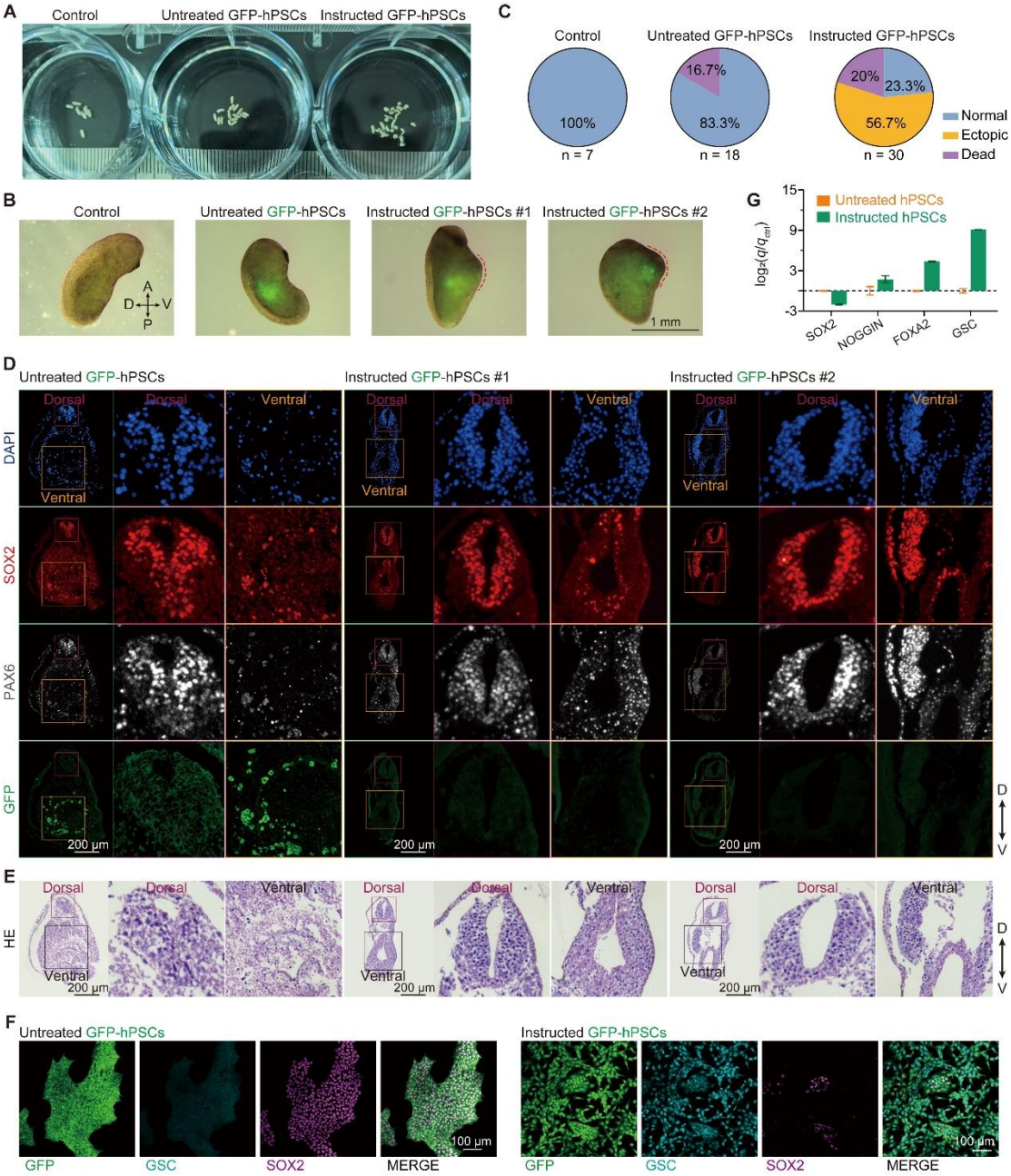

(A) *Xenopus* embryos subjected to transplantation experiments.
(B) *Xenopus* embryos transplanted with CHIR/Activin A-instructed GFP-hPSC exhibit ventral axis elevation (red dashed line) compared to untreated hPSC or control embryos.
(C) Quantification of dead, normal, and ectopic embryos following transplantation.
(D) IF showing SOX2 and PAX6 expression in the transversal section of *Xenopus* embryo.
(E) HE imaging of the transversal section of *Xenopus* embryos.
(F) IF showing GSC and SOX2 expression in untreated or instructed GFP-hPSC.

(G) qPCR analysis of the expression of the indicated genes.

Figure S2. Control experiments for the assembly model

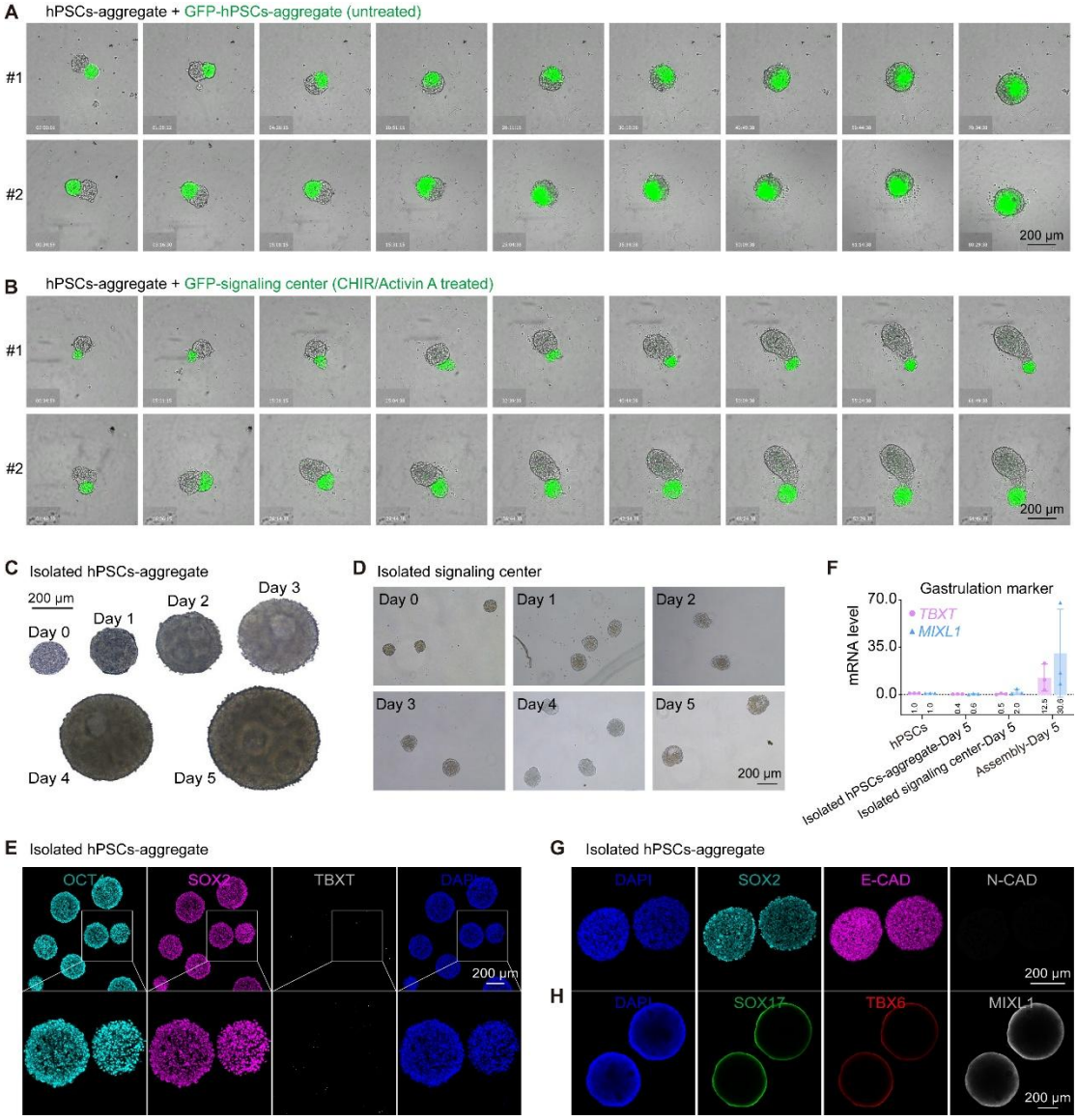

(A-D) Morphogenesis of the assembly of hPSC aggregates with untreated (A) or CHIR/Activin A treated (signaling center, B) GFP-hPSC aggregates, related to Video S1, and isolated cultured hPSC aggregates (C) and signaling center (D).

(E) IF showing expression of OCT4, SOX2 and TBXT.

(F) qPCR analysis of the expression of the indicated genes.

(G-H) IF showing expression of the indicated markers in isolated cultured hPSC aggregates.

Figure S3. Batch-to-batch reproducibility of gastruloid formation

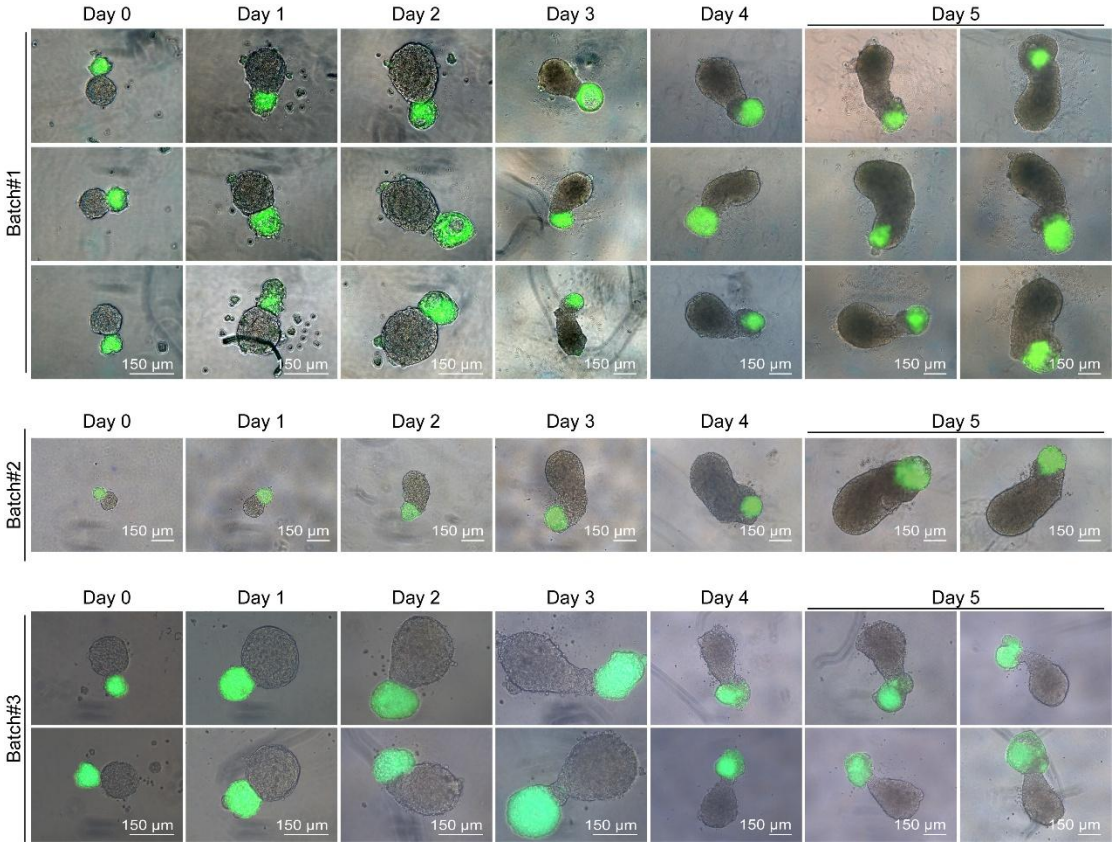

Representative images of gastruloids generated from multiple independent experimental batches, demonstrating consistent morphology and developmental features across batches.

Figure S4. Detection of gastrulation-relevant development in gastruloid

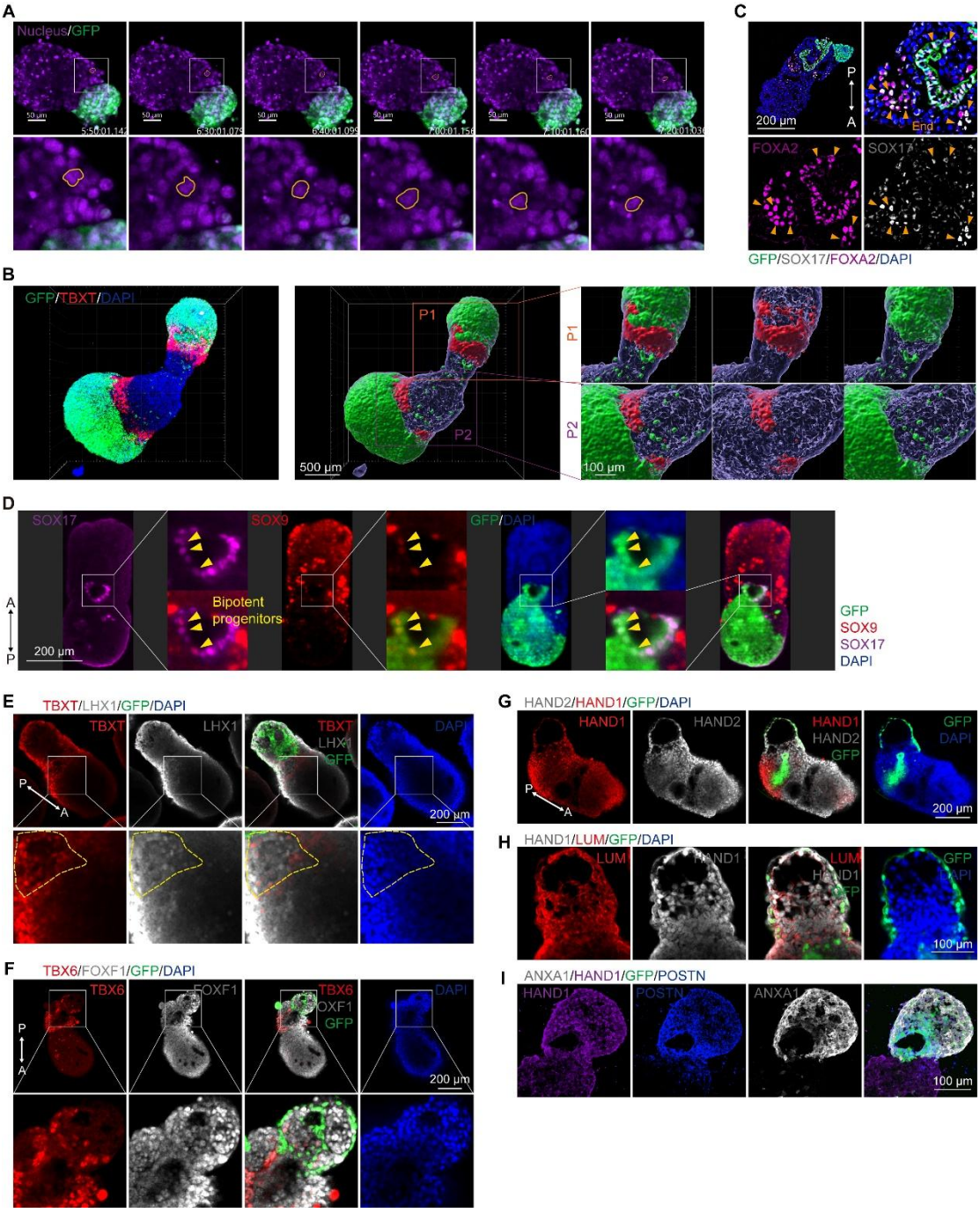

(A) Live cell imaging of gastruloid, related to Video S2. The yellow solid line indicates typical ingressed cells.

(B) IF showing expression of TBXT in dual GFP-signaling center assemblies.

(C) Representative IF images showing endodermal cells (SOX17/FOXA2).

(D) Representative IF images showing bipotent progenitors (SOX17/SOX9).

(E) Representative IF images showing TBXT and LHX1 expression in gastruloid.

(F) Representative IF images showing TBX6 and FOXF1 expression in gastruloid.

(G) Representative IF images showing HAND1 and HAND2 expression in

gastruloid.
(H) Representative IF images showing HAND1 and LUM expression in the gastruloid tail.
(I) Representative IF images showing ANXA1, HAND1, and POSTN expression in the gastruloid tail.

Figure S5. Replicates of gastruloids generated using different hPSC lines

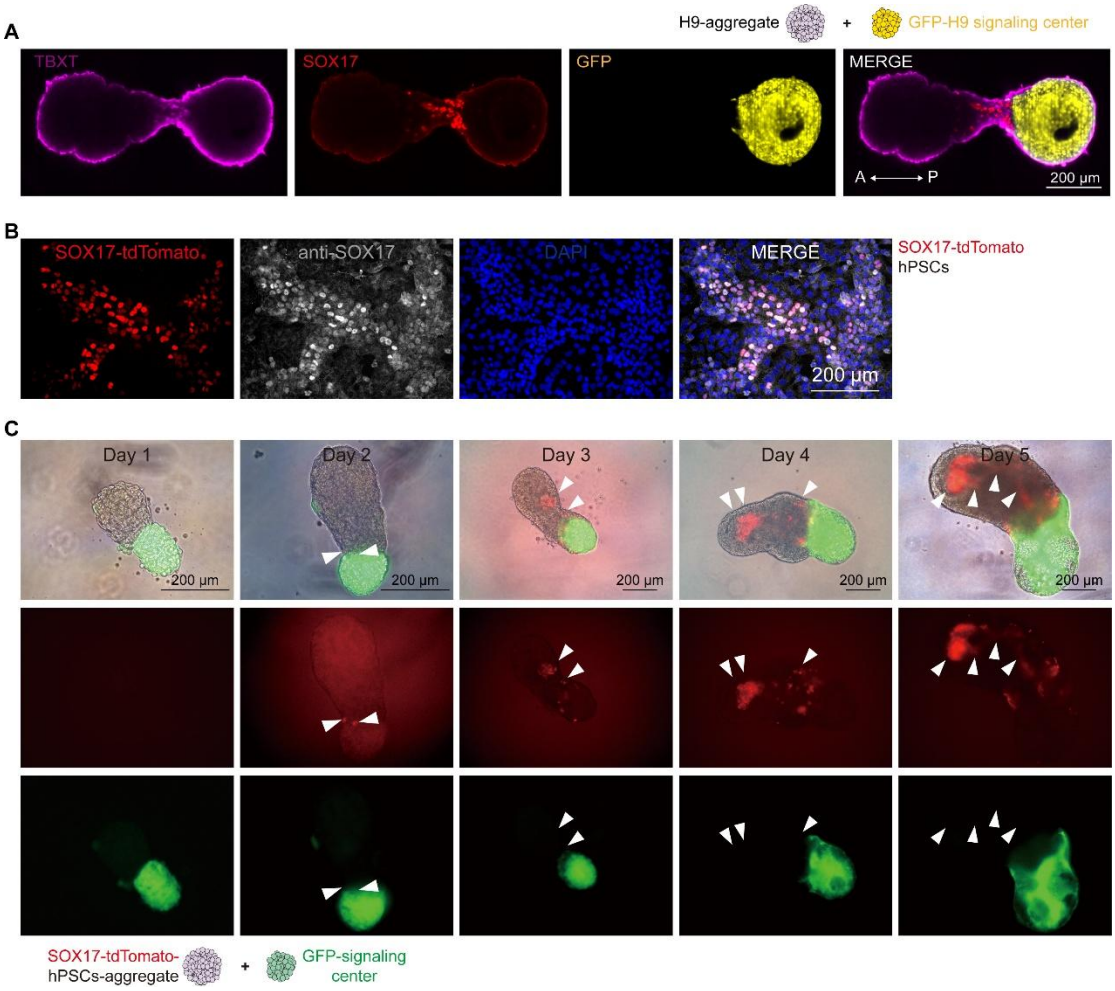

(A) Representative IF images showing TBXT and SOX17 expression in the H9-gastruloid.

(B) Representative IF images showing co-localization of SOX17-tdTomato and anti-SOX17 in SOX17-tdTomato RUES2 following endodermal differentiation.

(C) Morphogenesis of a gastruloid formed by assembling a SOX17-tdTomato RUES2-aggregate with a GFP-signaling center. The white arrow indicates SOX17-tdTomato-positive cells, representing endoderm.

Figure S6. Single-cell RNA-seq analysis of gastruloids, related to Fig. 3

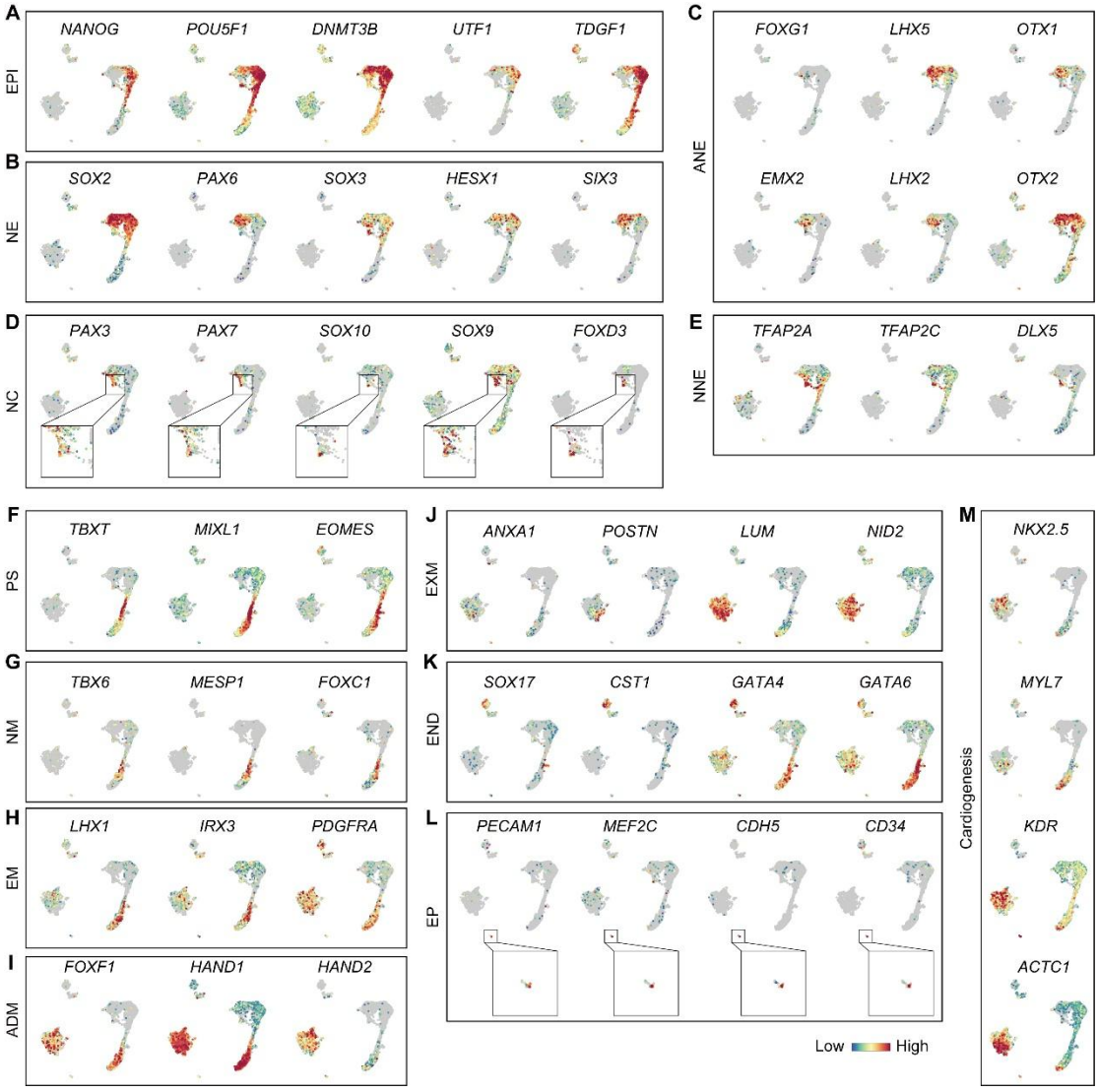

UMAPs displaying marker gene expression in the corresponding lineages found in day 5 gastruloids. EPI, epiblast; NE, neural ectoderm; ANE, anterior neural ectoderm; NC, neural crest; NNE, non-neural ectoderm; PS, primitive streak; NM, nascent mesoderm; EM, emergent mesoderm; ADM, advanced mesoderm; EXM, extraembryonic mesenchyme; END, endoderm; EP, endothelial progenitors.

Figure S7. Single-cell RNA-seq comparisons between gastruloids with monkey/mouse gastrulating embryos

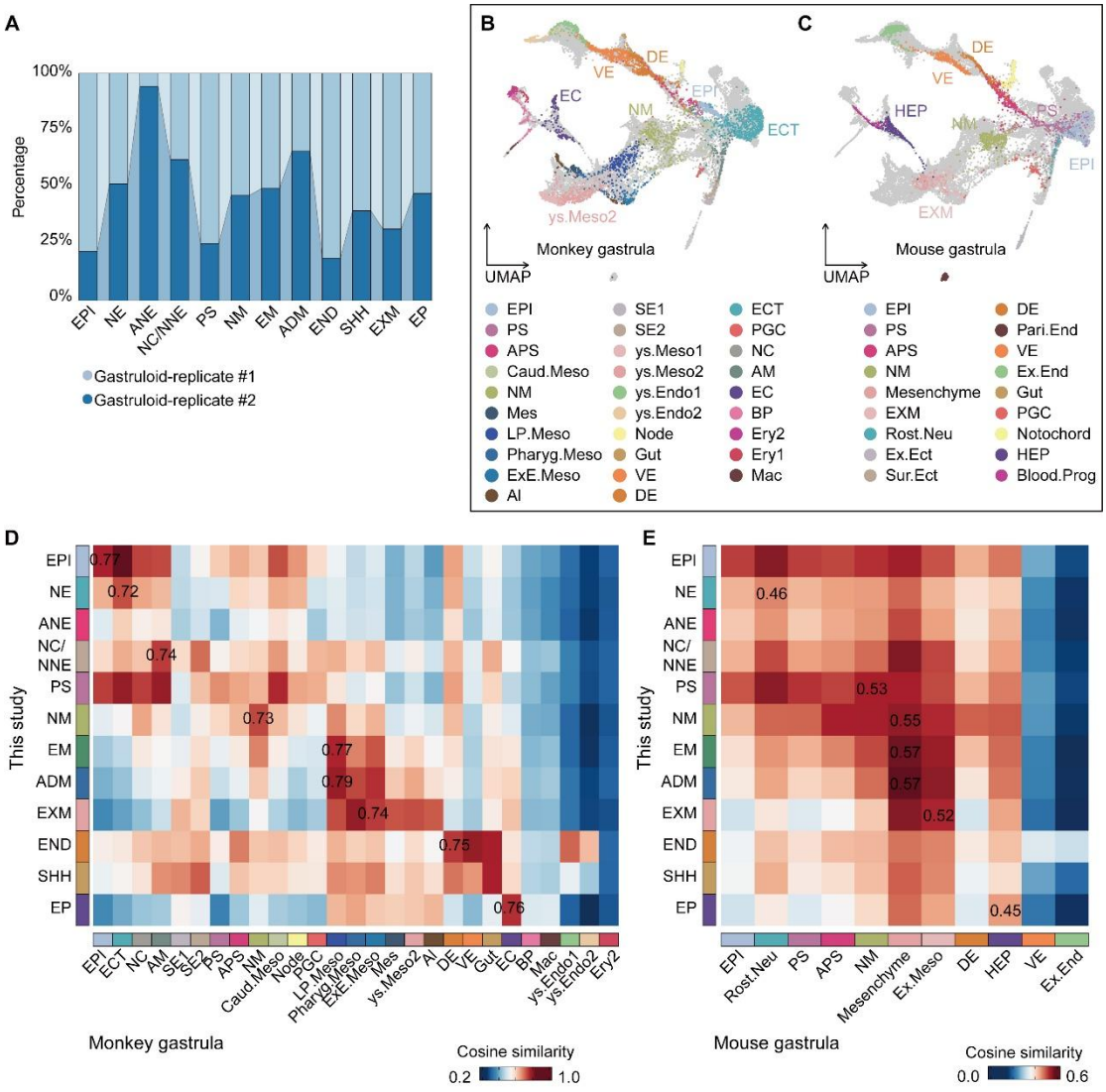

(A) Cell proportions in gastruloids from two independent experiments.

(B-C) UMAPs showing the integration of day 5 gastruloids with reference cells from monkey (B) and mouse (C) gastrulas. EPI, epiblast; PS, primitive streak; APS, anterior primitive streak; Caud.Meso, caudal mesoderm; NM, nascent mesoderm; Mes, mesenchyme; LP.Meso, lateral plate mesoderm; Pharyg.Meso, pharyngeal mesoderm; ExE.Meso, extraembryonic mesoderm; AI, allantois; SE1/2, surface ectoderm1/2; ys.Meso1/2, yolk sac mesoderm1/2; ys.Endo1/2, yolk sac endoderm1/2; VE, visceral endoderm; DE, definitive endoderm; ECT, ectoderm; PGC, primordial germ cells; NC, neural crest; AM, amnion; EC, endothelial cell; BP, blood progenitor; Ery1/2, erythrocyte1/2; Mac, macrophage; Rost.Neu, rostral neuroectoderm; Ex.Ect, extraembryonic ectoderm; Sur.Ect, surface ectoderm; Pari.End, parietal endoderm; Ex.End, extraembryonic endoderm; Blood.Prog, Blood progenitors.

(D-E) Similarity heatmap comparing expression profiles of cell lineages

between gastruloids and monkey (D) or mouse (E) gastrula.

Figure S8. Single-cell RNA-seq comparisons between gastruloids and other stem cell-based embryo models

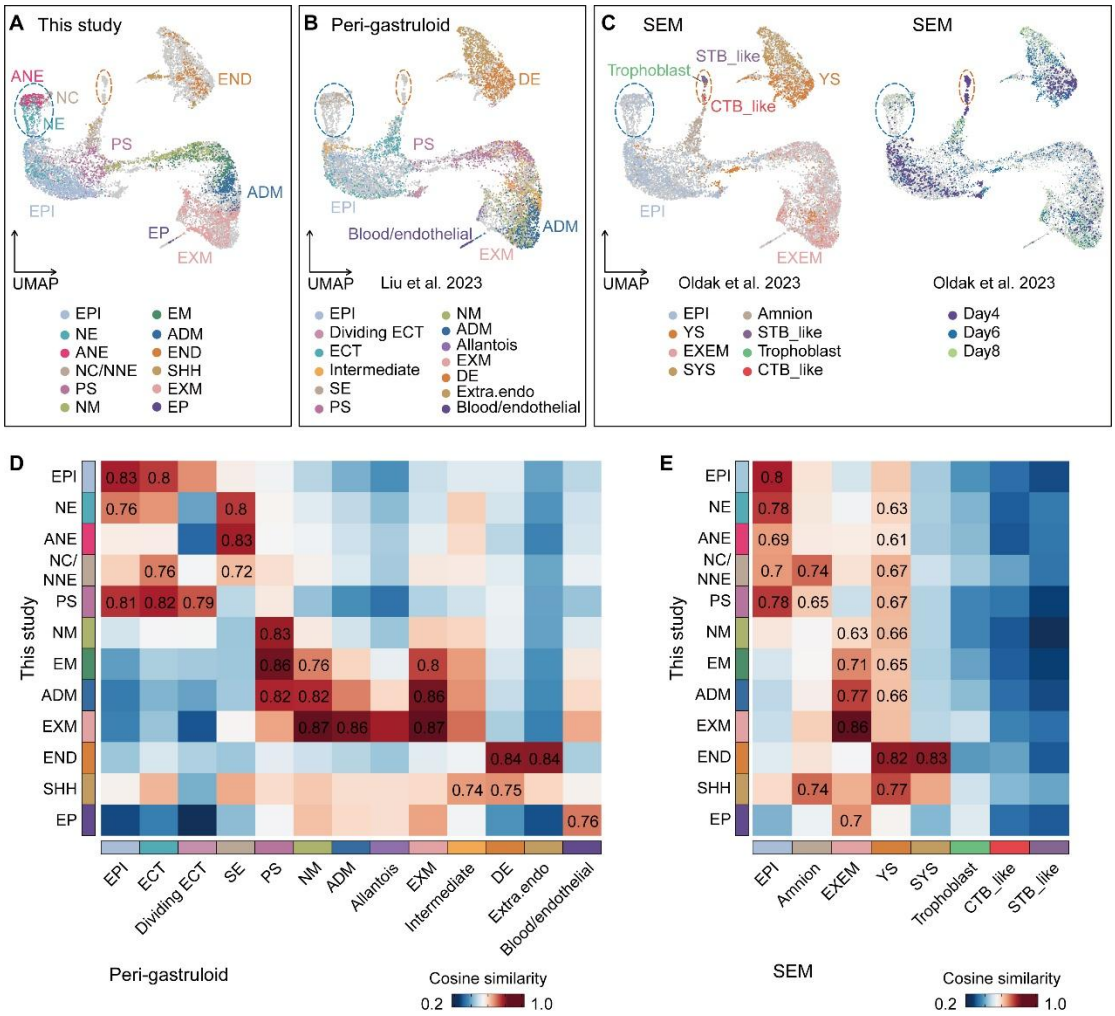

(A-C) UMAPs showing integration of day 5 gastruloids (A) with reference peri-gastruloid (B) and synthetic embryos model (SEM) cells (C). DE, definitive endoderm; Extra.endo, extraembryonic endoderm; Intermediate, intermediate cell types; SE, surface ectoderm; YS, yolk sac; SYS, secondary yolk sac; CTB-like, cytotrophoblast-like cells; STB-like, syncytiotrophoblast-like cells.
(D-E) Similarity heatmap comparing expression profiles of cell lineages between our gastruloid and peri-gastruloid (D) or SEM (E).

Figure S9. The BMP signaling pathway is involved in gastruloid development

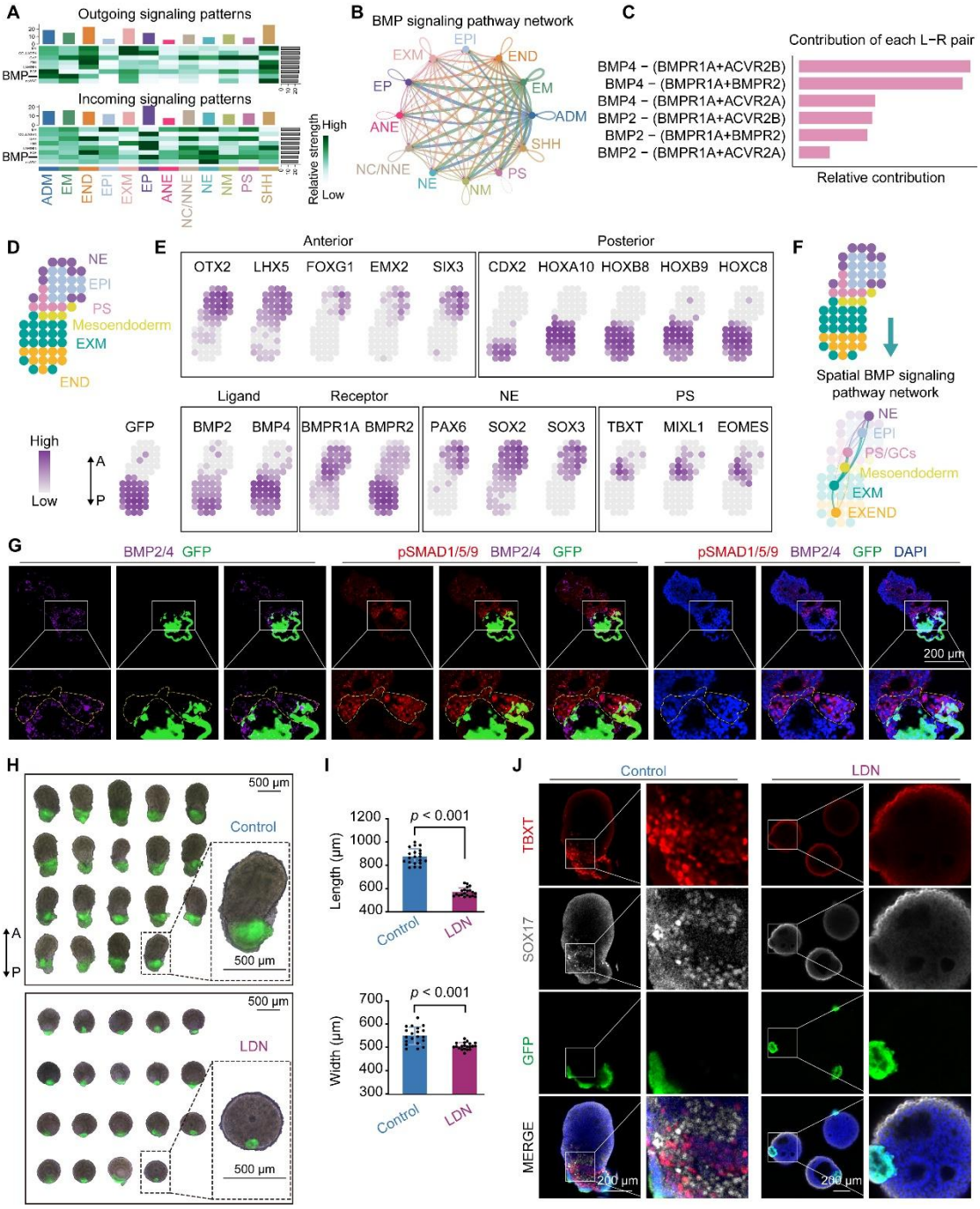

(A) Heatmap depicting the relative importance of cell-cell interactions across different cell types.

(B) Analysis of cell-cell communication networks specific to BMP signaling among various cell types.

(C) GO analysis predicting the major BMP ligand-receptor pairs.

(D) Unsupervised spatially constrained clustering of a representative gastruloid. NE, neural ectoderm; EPI, epiblast; PS, primitive streak; EXM, extraembryonic mesenchyme; END, endoderm.

(E) Spatial expression patterns of key representative genes.
(F) Spatial network of the BMP signaling pathway.
(G) IF images of BMP2/4 and phosphorylated SMAD1/5/9 (pSMAD1/5/9) in gastruloid.
(H, I) Morphological effects of BMP pathway inhibition on gastruloids. (H) Bright-field images of day 5 gastruloids treated with the BMP inhibitor LDN193189 (LDN) or control. (I) Quantification of gastruloid length and width. Data are presented as mean ± SD (Control, n = 20; LDN, n = 20).
(J) IF staining of TBXT and SOX17 in control and LDN-treated gastruloids.

Figure S10. The specification of neural tissues in gastruloid

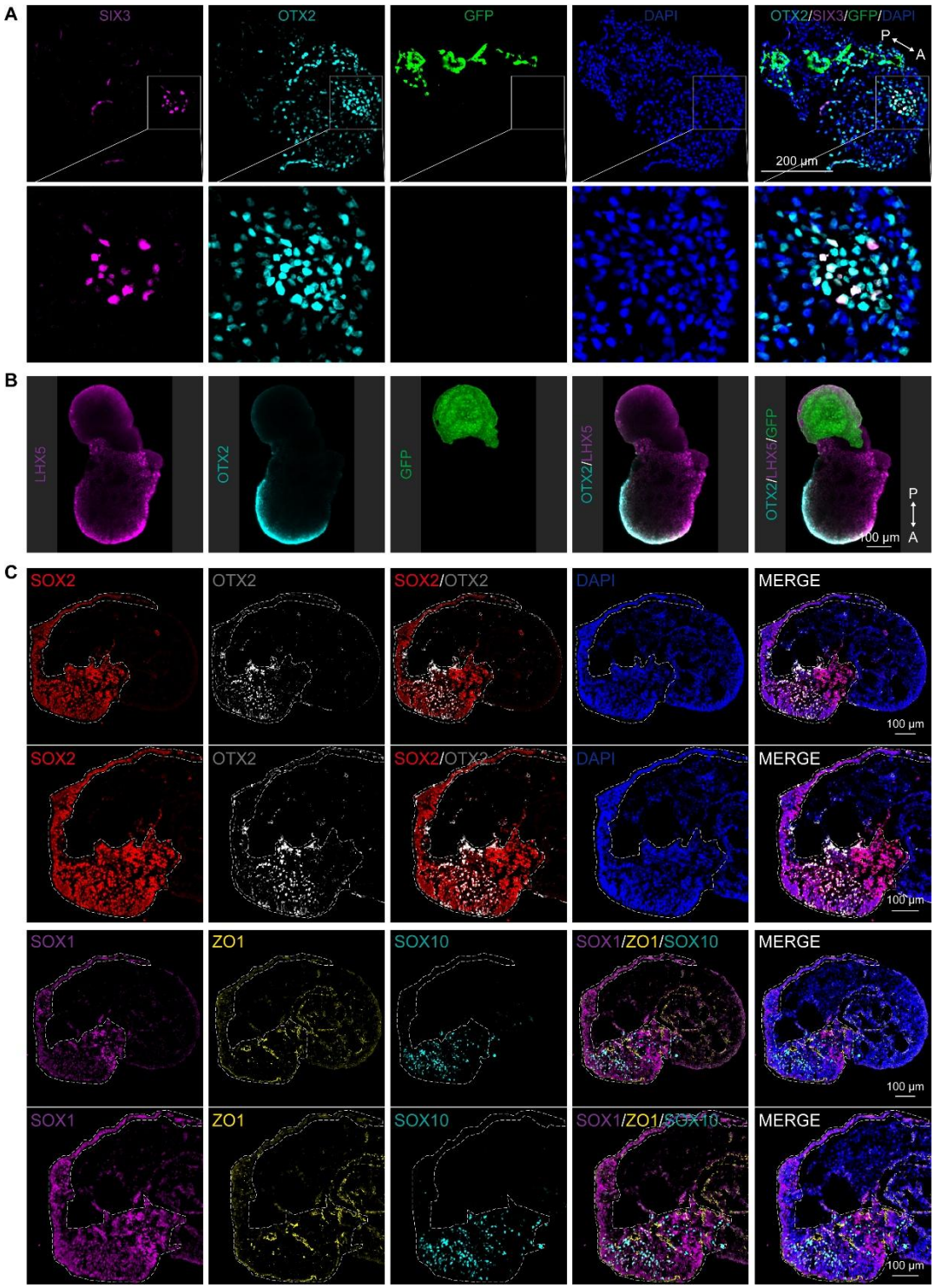

(A) Representative IF images showing SIX3 and OTX2 expression in day 5 gastruloid.

(B) Representative IF images showing LHX5 and OTX2 expression in day 5 gastruloid.

(C) Representative IF images showing SOX2, OTX2, SOX1, ZO1, and SOX10 expression in day 5 gastruloid.

Figure S11. The presence of neural mesodermal progenitor (NMP)-like cells in gastruloid

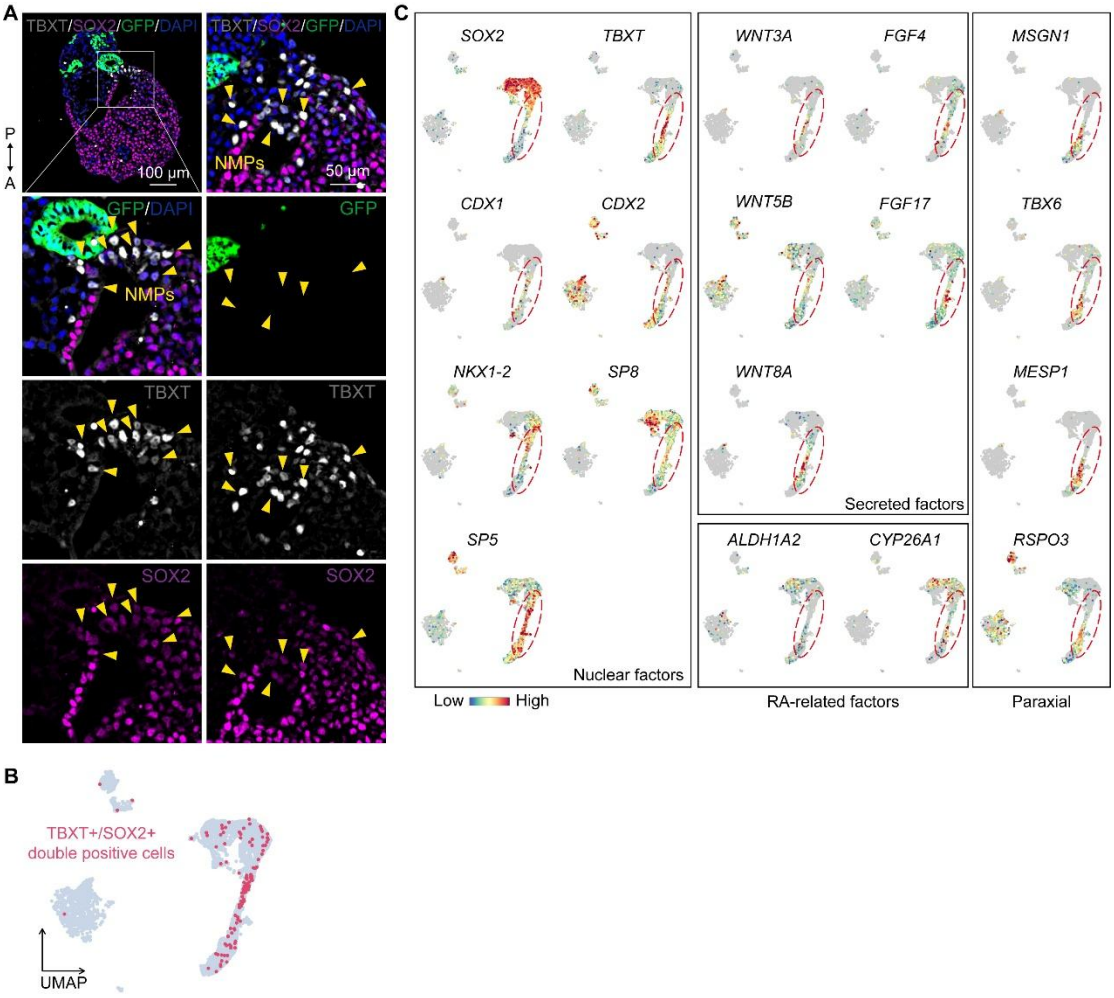

(A) Representative IF images showing TBXT and SOX2 double-positive cells, indicating neuromesodermal progenitors-like cells (NMPs-like cells, marked with yellow triangles).

(B) UMAPs highlighting *TBXT*/*SOX2* double-positive cells (red dots).

(C) UMAPs displaying the expression of marker genes in day 5 gastruloids.

Figure S12. SHH and antagonistic BMP signal in gastruloids

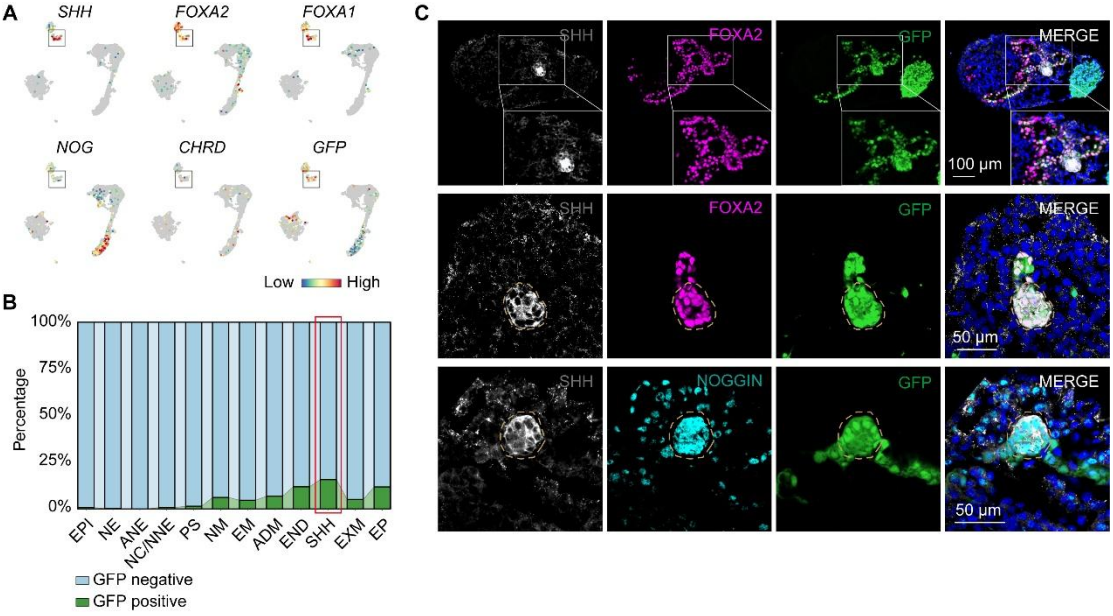

(A) UMAPs displaying the expression of marker genes in SHH-positive cells.
(B) Proportions of GFP mRNA-positive cells across different cell types.
(C) Representative IF images showing SHH, FOXA2, and NOGGIN expression in day 5 gastruloids.

Figure S13. Batch-to-batch reproducibility of PANPAN development

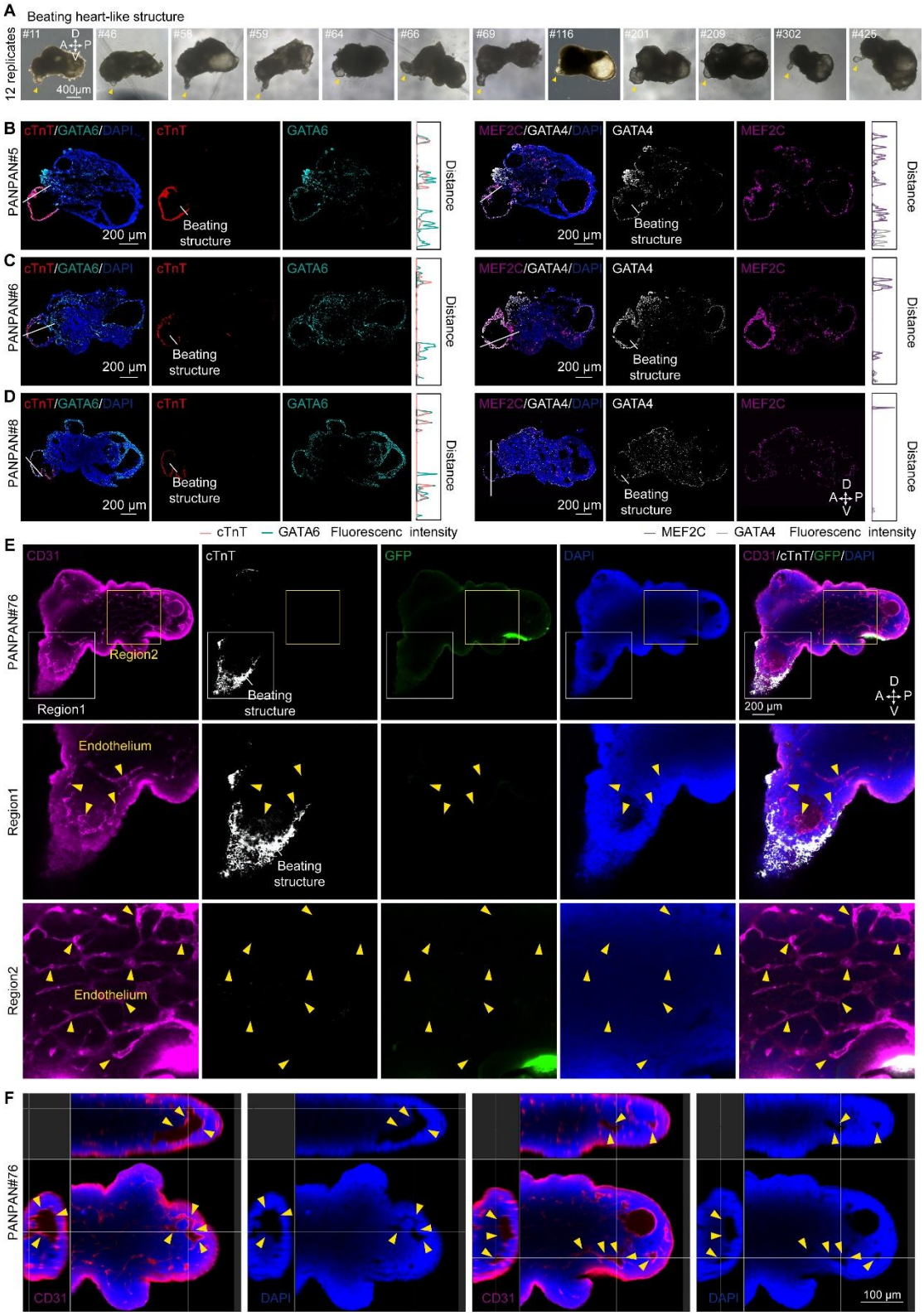

(A) Representative samples of PANPAN, with yellow arrows indicating the beating structure, related to video S5.

(B-F) IF staining showing cardiac (cTnT, GATA6, GATA4, and MEF2C) and endothelial marker (CD31) in PANPANs. Yellow arrows indicate the lumenized structures within CD31-positive endothelial-associated networks (F).

Figure S14. Anterior neural tissues and endodermal pocket in PANPAN

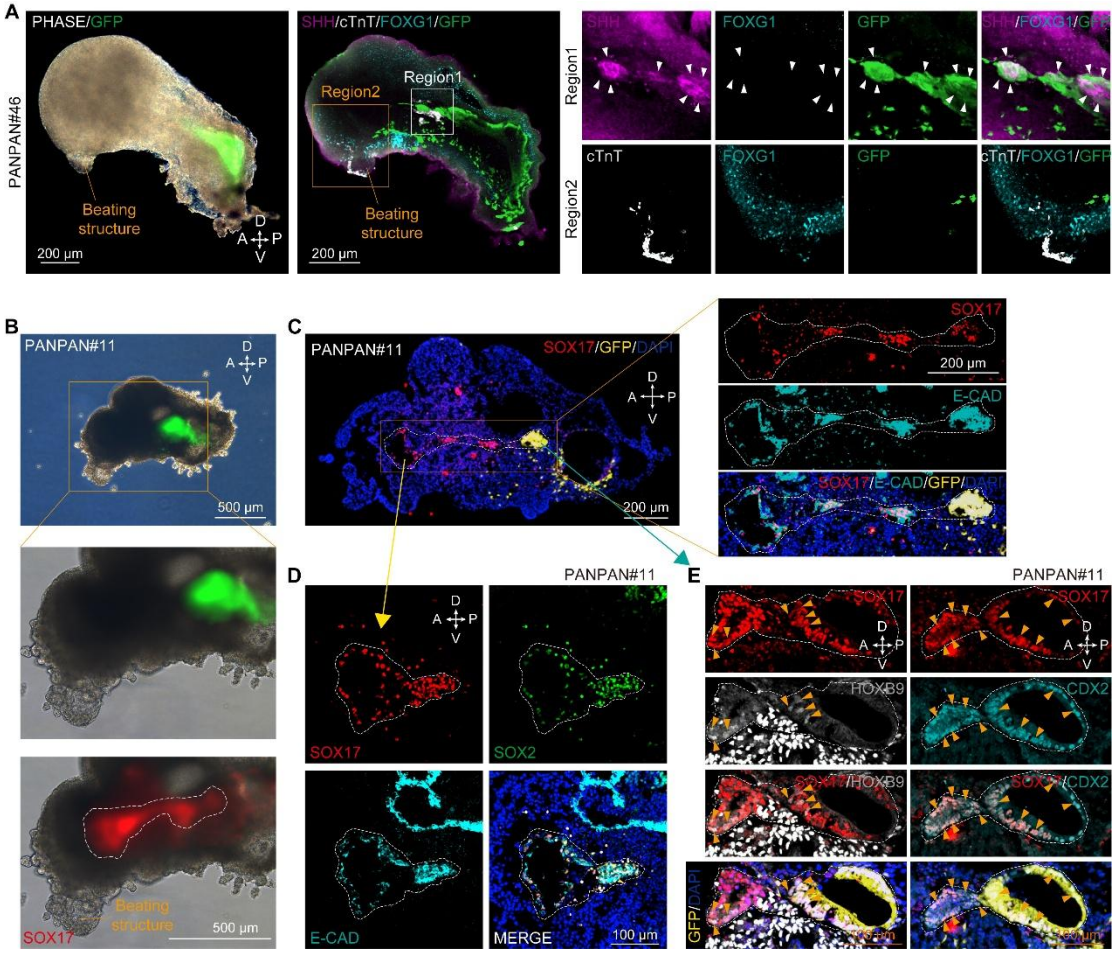

(A) IF images showing brain marker FOXG1, cardiac marker cTnT, SHH, and GFP.

(B) Representative merged fluorescence and brightfield images of PANPAN#11. White lines outline a SOX17-positive spanning structure.

(C) IF staining showing expression of the epithelial marker E-CAD in the SOX17-positive spanning structure.

(D) IF staining showing SOX17, SOX2, and E-CAD expression in the anterior pocket.

(E) IF staining showing SOX17, HOXB9, and CDX2 expression in the posterior pocket.

Figure S15. Single-cell RNA-seq analysis of PANPAN

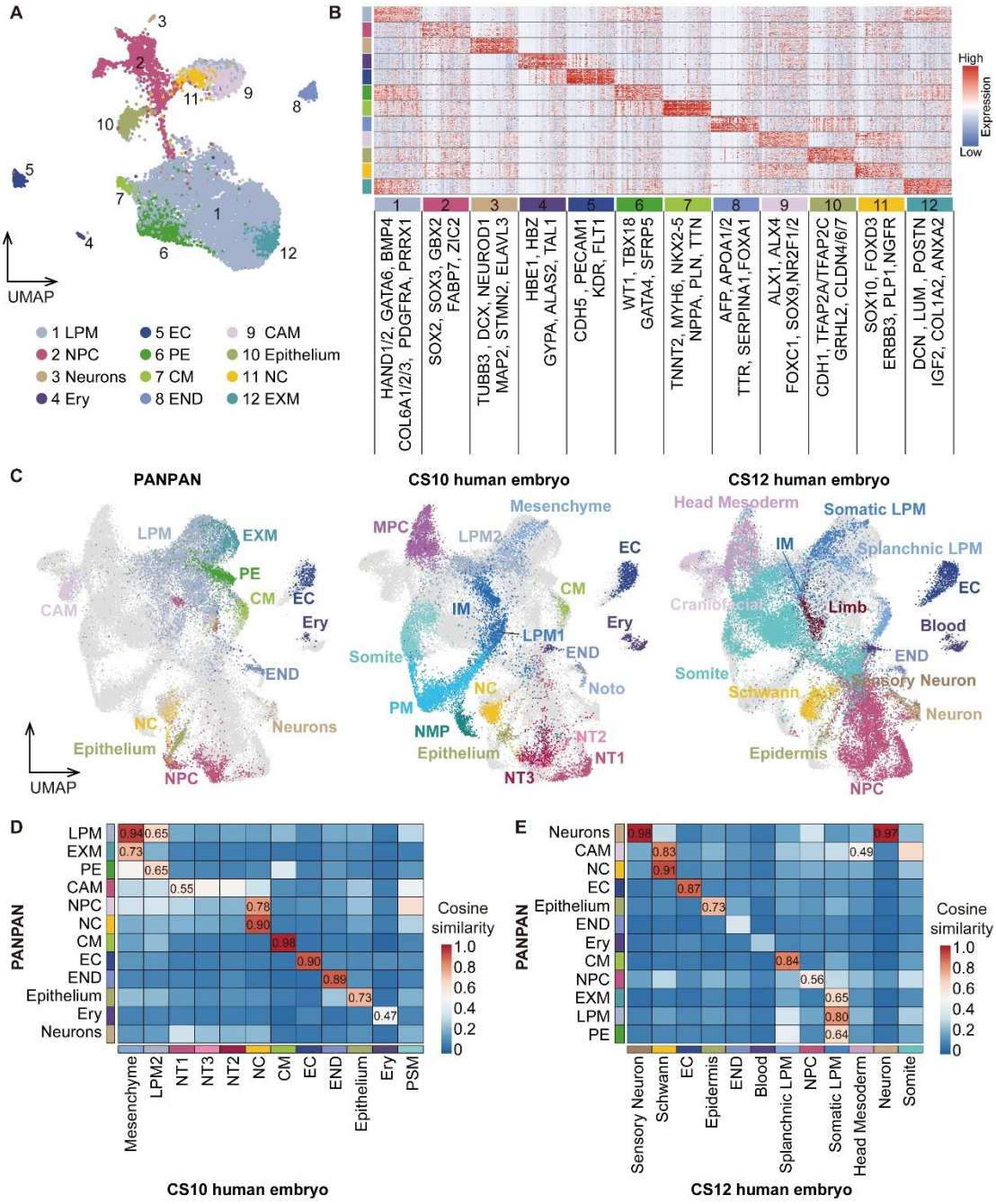

(A) UMAP visualization representing individual cells derived from PANPANs (beating gastruloids). Twelve distinct colored clusters are identified, corresponding to different cell types: LPM, lateral plate mesoderm; NPC, neural progenitor; Neurons; Ery, erythroid cell; EC, endothelial cell; PE, proepicardium/epicardium; CM, cardiomyocytes; END, endoderm; CAM, cranial mesenchyme; Epithelium; NC, neural crest; EXM, extraembryonic mesenchyme.

(B) Heatmap displaying the top 50 differentially expressed genes (DEGs) for each cluster shown in (A).

(C) UMAPs showing the integration of PANPAN (left) with reference CS10 (middle) and CS12 (right) human embryo-originated cells.
(D-E) Similarity heatmap comparing expression profiles of cell lineages between PANPAN with CS10 (D) or CS12 (E) human embryos.

Figure S16. Generation of multiple potential signaling centers in hPSC treated with different combinations of BMP, WNT, and NODAL signaling

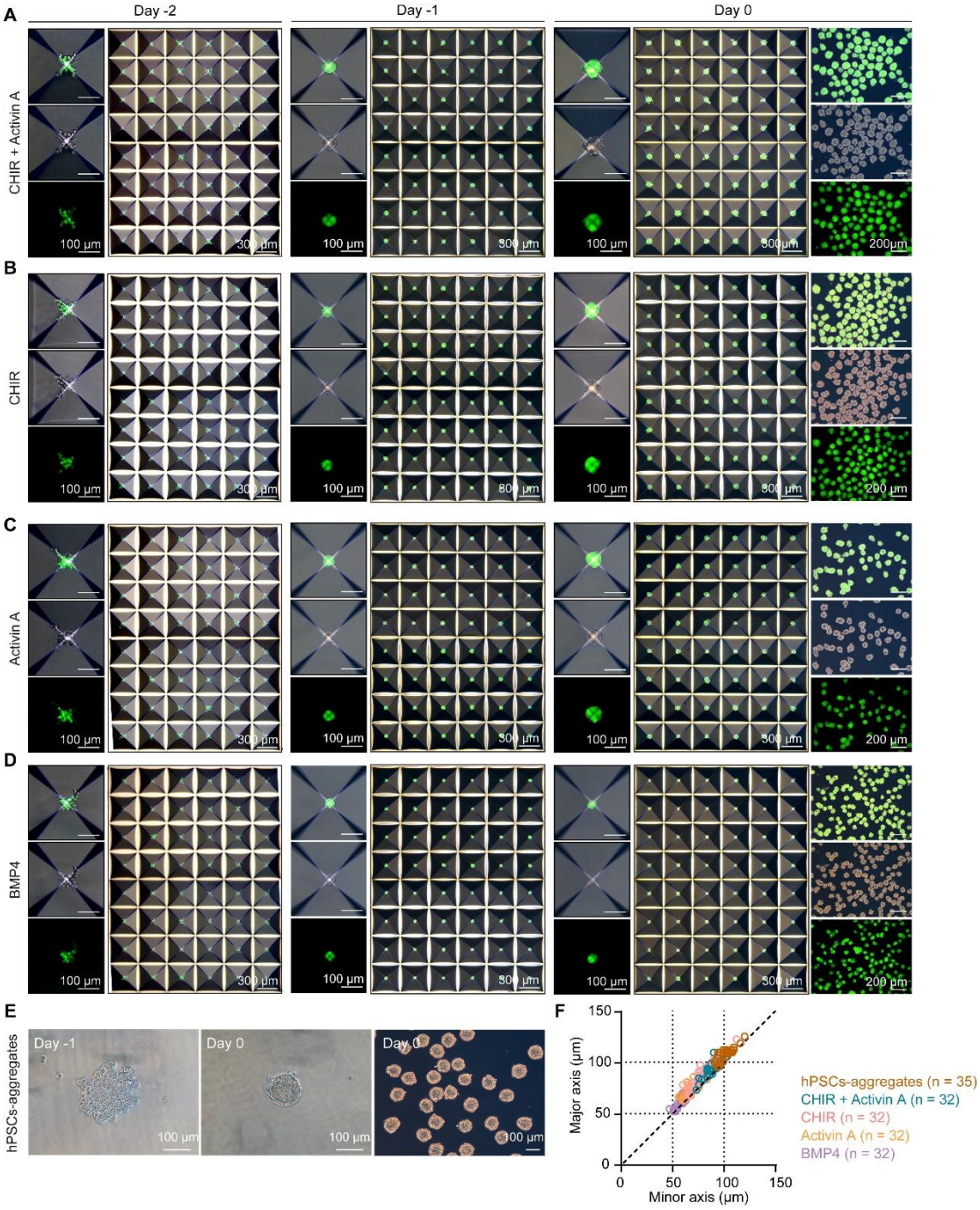

(A-D) Time-course development of GFP-hPSC treated with CHIR + Activin A (A), CHIR alone (B), Activin A alone (C), or BMP4 alone (D).

(E) Time-course formation of hPSC aggregates.

(F) Measurements of the major and minor axes of aggregates corresponding to panels (A-E).

Figure S17. Formation of multiple assembloids by pairing hPSC aggregates with different signaling centers

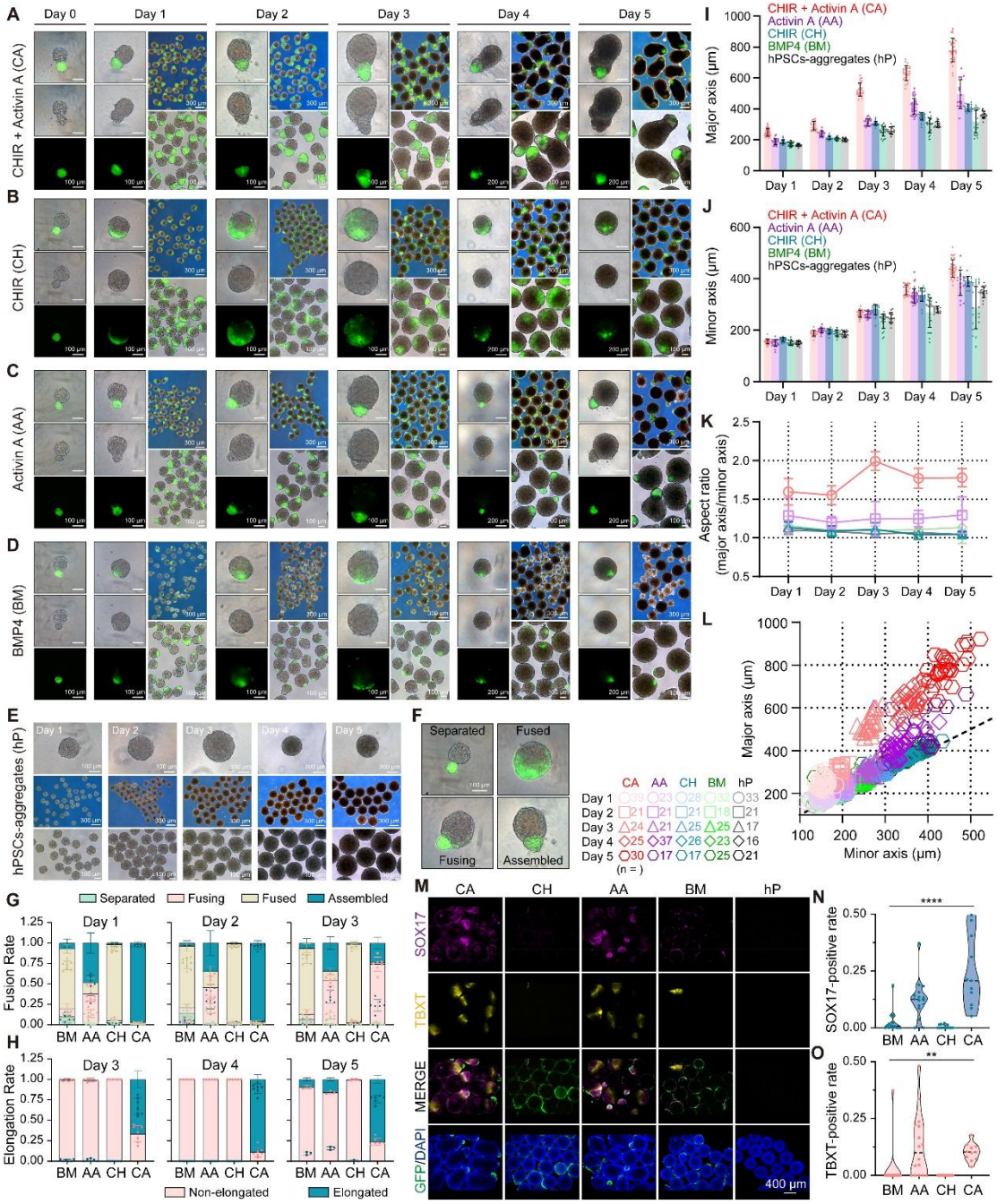

(A-E) Time-course development of assembloids paired with treated signaling centers (A–D) and aggregates cultured alone (E).

(F) Typical features of separated, fusing, fused, and assembled states.

(G-L) Integration (G), elongation (H), axes measurements (I, J, and K), and aspect ratio (K) were quantified.

(M) IF staining of SOX17 and TBXT in multiple assembloids.

(N-O) Quantification of the percentage of SOX17-positive (N) and TBXT-positive cells (O). ****P < 0.0001, **P < 0.01.

Figure S18. RNA-seq analysis of multiple potential signaling centers

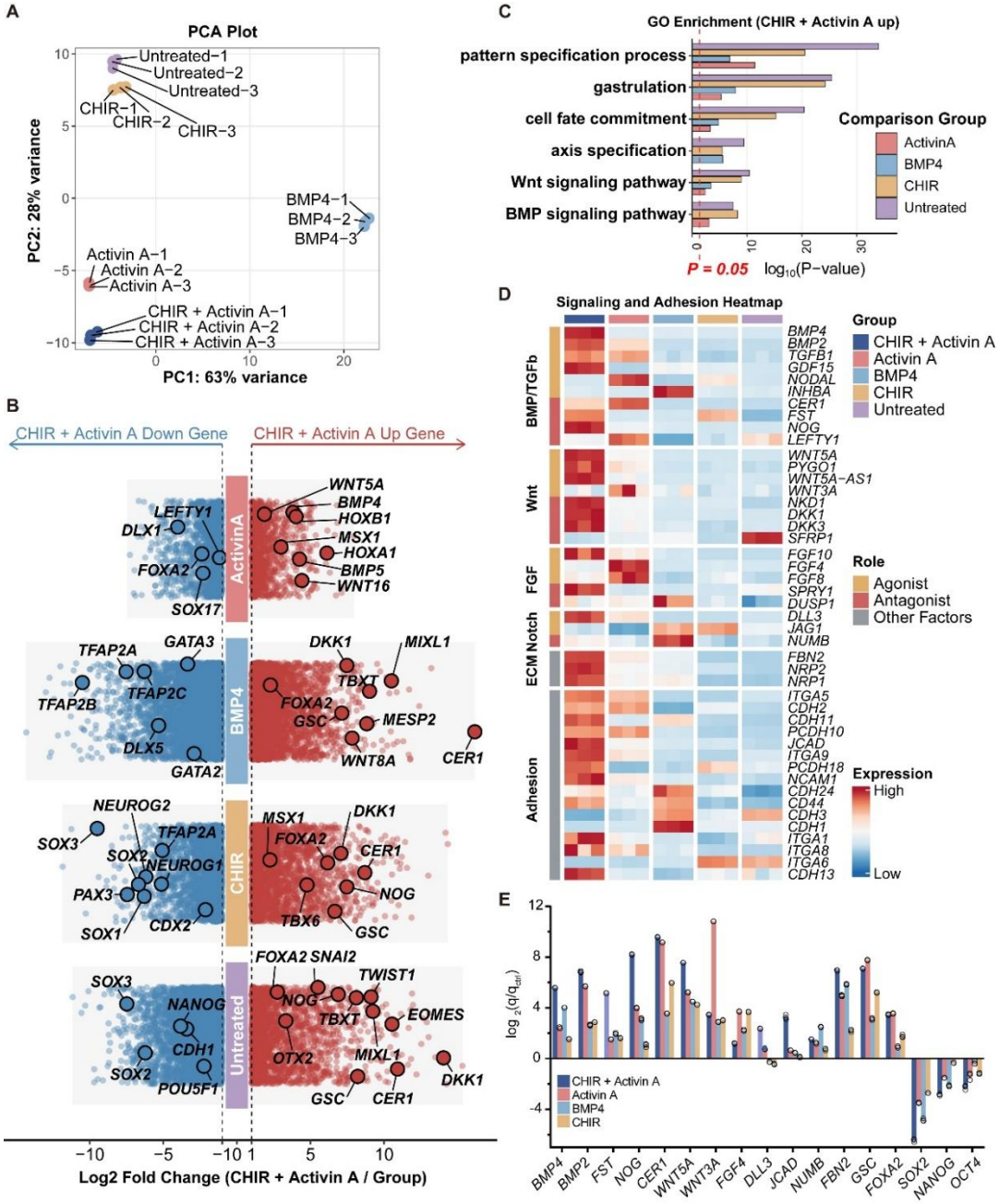

(A) Principal component analysis (PCA) of bulk RNA-seq data from different signaling center conditions.

(B) Volcano plots comparing gene expression profiles of different signaling centers with the CHIR + Activin A group, highlighting key upregulated and downregulated genes.

(C) Gene Ontology (GO) enrichment analysis of genes upregulated in the CHIR + Activin A group.

(D) Heatmap showing the expression levels of key factors involved in major signaling pathways across multiple potential signaling centers.

(E) qPCR validation of selected key factors.

Supplemental table of oligonucleotides

Table S1.
Primers used for quantitative PCR

Gene	Forward primer (5'-3' orientation)	Reverse primer (5'-3' orientation)
GSC	AACGCGGAGAAGTGGAACAA	AGCATCGTCTGTCTGTGCAA
FOXA2	GGAACACCACTACGCCTTCAAC	AGTGCATCACCTGTTCGTAGGC
NOGGIN	GAAGCTGCGGAGGAAGTTAC	TACAGCACGGGGCAGAAT
MIXL1	CAAGTCTCGGCGTCAGAGTG	GGCAGGCAGTTCACATCTAC
TBXT	AAGAACGGCAGGAGGATGTT	GACTTTGCTGAAGGAGACGG
GAPDH	CACCGTCAAGGCTGAGAACG	TTGCTGATGATCTTGAGGCTGT

Supplemental videos

Video S1.
Morphogenesis of the assembly of hPSC aggregates with untreated (top) or CHIR/Activin A treated (signaling center, bottom) GFP-hPSC aggregates.

Video S2.
Live cell imaging of gastruloid. The yellow solid line indicates typical ingressed cells.

Video S3.
PANPAN#11 exhibited a beating chamber.

Video S4.
Three beating PANPANs.

Video S5.
Representative samples of PANPAN, with yellow arrows indicating the beating chambers.

Video S6.
Calcium imaging of a beating domain using a Calbryte™ dye.